DOI: 10.13009/EUCASS2017-206

Simulation of Fluid Structure Interaction in Overexpanded Cold Gas Rocket Nozzles using the DLR TAU Code

Sebastian Jack⋆ and Michael Oschwald†
⋆DLR German Aerospace Center, Institute of Aerodynamics and Flow Technology
Braunschweig, Germany, D-38108
†DLR German Aerospace Center, Institute of Space Propulsion
Lampoldshausen, Germany, D-74239

Abstract

During the transient startup and shutdown process of a rocket engine high side loads occur, due to unsymmetrical flow patterns. The resulting deformation, and its retroactive effect onto the internal flow, may excite the nozzle structure and can lead to its fatal damage. Flow separation at the nozzle wall amplifies the deformation. To investigate and predict the effects and the underlying mechanisms a simulation environment, coupling the DLR TAU code to the structural analysis tool MSC Nastran, was used to simulate the flow structure interaction and its scalability in sub-scale cold gas rocket engine nozzles.

Nomenclature

Symbols

δ	analogue thickness
ε	expansion ratio
Φ	normalized eigenfrequency
Λ	logarithmic decrement
m	circumferential wave number
n	axial wave number
p	pressure
R	local nozzle contour radius
t	time
t_w	wall thickness
T	temperature
W	work the fluid performs on the structure
X	axial coordinate, main flow direction

Indices

$*$	nozzle throat
a	ambient condition
div	divergent nozzle section
sep	flow separation
tot	total
w	wall

Abbreviations

CFD	computational fluid dynamics
CSM	computational structural mechanics
FFT	fast Fourier transformation
GCI	grid convergence index
GFP	glass-fiber reinforced plastic
NPR	nozzle pressure ratio
RANS	Reynolds-averaged Navier Stokes euqations
RSM	Reynolds stress turbulence model
TIC	truncated ideal contour
TIC-53	used TIC nozzle with design Mach number of 5.3 (see Genin et al[9])

1. Introduction

Geometrical and transient imperfections, such as an asymmetrical flow, combustion instabilities or the flow around the launcher's body during its ascend (buffeting), deform the structure of a rocket engine nozzle during its operation. For a full flowing nozzle, i.e. when the pressure in the combustion chamber is high enough to ensure a supersonic flow within the complete nozzle up to its exit plane, the change of the structural loads caused by a local change of the wall pressure counteracts this initial deformation. The interaction between the nozzles inner flow and its structure damps the system's excitation. During the start-up and shut-down process of the engine, as well as for a highly reduced thrust

DOI: 10.13009/EUCASS2017-206

level that can be desirable to adjust the launcher's trajectory to a desired target, flow separation might occur within the nozzle. For these highly overexpanded modes of operation a subsonic flow region with large pressure gradients is present in the rear outer region of the flow which is sensitive to changes in the inflow conditions and nozzle contour. In this case the aforementioned initial deformations can be enhanced by the fluid structure interaction and excite the nozzles eigenmodes. These mechanisms, that are described in detail by several authors,[5,8,19] can induce high side loads and lead to fatal damages. A detailed investigation of the nozzles loads is therefore relevant for the dimensioning process. A better understanding of these processes could help to improve the dimensioning of overexpanded rocket nozzles and thus the performance of future launcher systems. To understand the underlying phenomena and develop a validated numerical model the process of nozzle deformation has been investigated in the DLR internal cooperation project ProTAU and its ongoing successor TAUROS. One of its main goals is to reproduce the relevant effects in subscale experiments that can be performed on a testbench environment.

2. Computational method

To simulate the unsteady interaction between the internal separated flow within a rocket engine nozzle and the deformation of its structure, a tightly coupled partitioned method between the computational fluid dynamics code DLR-TAU and the structural analysis software MSC Nastran has been extended. A description of the basic method, including its validation for panel flutter test cases, was published by Alder.[1] This method has been enhanced to meet the requirements of a nozzle simulation, e.g. the interpolation of inner and outer forces and the conservation of the structure's wall thickness.

2.1 CFD solver

The DLR-TAU code was used to simulate the flow within the computational domain of the nozzle. TAU is a finite volume solver that solves the instationary Reynolds-averaged Navier Stokes equations (RANS). For comparability to earlier simulations[9,12] and experimental data[7,8] Nitrogen as perfect gas was used as fluid model. To close the equation system a Reynolds stress (RSM) turbulence model was used, which has proven to perform well for the simulation of separated flows in cold gas nozzles.[9,11,12] The used RSM consists of the Wilcox stress-ω model as re-distribution model,[14] the isotropic model by Rotta as dissipation model,[22] a diffusion model based on the generalized gradient diffusion hypothesis by Daly and Harlow,[4] and the necessary length scale computed on basis of the Menter baseline ω-equation.[15] An upwind scheme is applied for the flux vector splitting in space, using gradient reconstruction to achieve second order accuracy. The Second order accurate dual-time-stepping scheme by Jameson[13] is used for time integration. All calculations have been performed on hybrid grids of the full rotation-symmetric nozzle geometry to avoid symmetric effects forced by internal boundary contitions.

2.2 CSM solver

All presented results have been computed using the structural mechanics solver Nastran that has originally been developed by NASA in the 1960's and is widely used for aerospace applications. The implicit non-linear solution process SOL400 of the commercial derivative MSC Nastran by MSC Software has been applied (for further information on this tool see the Nastran user guide[16]). This finite element method uses an implicit iterative Newton-Raphson method to compute the systems stiffness matrix and a second order accurate scheme by Hilber, Hughes and Taylor[10] for time integration. For all simulations the structure has been modeled using the assumption of thin quadrilateral shell elements.

2.3 Coupling

Interpolation

To couple the aforementioned single domain solvers they have to exchange state variables, i.e. load f and displacement d data, at the interface region of their non-overlapping meshes. Radial basis functions have been used to interpolate the deformation output onto the fluid mesh. This method is widely spread among aeroelastic applications due to its conservation properties and well described by Neumann.[17] Since two dimensional shell elements are used to model the nozzle structure, the applied interpolation routines were modified to ensure conservation of the wall thickness. At discontinuities, that are present in the load distribution due to the existence of an internal separation shock, this method leads to overshoots and therefore large interpolation errors. A nearest neighbour search, combined with a moment correction, is therefore applied to interpolate the aerodynamic loads to the structure mesh. Preliminary studies have shown that the interpolation errors are well below 0.2 % and hence negligible for the presented calculations.

DOI: 10.13009/EUCASS2017-206

Coupling scheme

Figure 1 shows a schematic description of the coupling procedure that is being applied to proceed from timestep t_i to t_{i+1}. In a first step the CFD solver computes the aerodynamic loads which are interpolated onto the structural domain (1). The CSM solver uses these as Neumann boundary conditions and computes the actual deformation data (2, predictor step) which are interpolated to the fluid domain (3) and set as Dirichlet boundary conditions in the latter. The CFD solver then proceeds to timestep t_{i+1} (4) and returns the updated loads to the CSM domain at the preceding timestep (5). Based on this updated information at least one corrector loop (dashed lines, analogue to 2, 3, 4) is calculated. The difference of the norm of the displacement vector of two consecutive inner loops is used as convergence criterion. For the presented results one or two corrector loops were sufficient to reach a residual of 1.0×10^{-3} for each timestep.

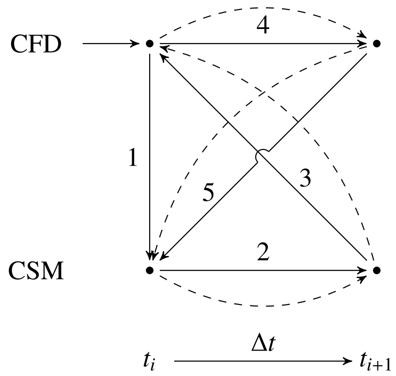

Figure 1: Schematic description of the coupling procedure

2.4 Boundary conditions and resolution

A sketch of the computational domain, including measurements and boundary conditions, is shown in figure 2. Besides the aforementioned exchange of state variables at the interface boundary, all boundary conditions remain invariant during the complete simulation, i.e. the coupled system is not exited externally. The inflow condition at the nozzle inlet (reservoir pressure inflow) assumes an isentropic expansion from a given total state (here $T_{tot} = 300\,\mathrm{K}$ and a varying total pressure p_{tot}). The total pressure at this boundary is used to alter the nozle pressure ratio NPR $= p_{tot}/p_a$. Up to an expansion ratio of $\varepsilon = 5.0$, i.e. $R = \sqrt{5}R^*$, the nozzles inner and outer wall are considered ideal stiff and therefore undeformed since in realistic engine configurations (e.g. Vulcain 2) this region is usually milled out of solid copper to house the necessary cooling channels. At this interface point the structure mesh is clamped, i.e. fixed in all six degrees of freedom.

The influence of the spatial resolution of the fluid domain onto the relevant flow quantities has been evaluated using the grid convergence index (GCI) proposed by Roache.[21] Since along discontinuities the CFD solver reduces the order of spatial gradient calculation to one to ensure numerical stability, $p = 1.75$ has been set for the necessary order of convergence as proposed by various authors and proven realistic for the TAU code by Rakowitz.[20] Since three spatial discretization stages have been used for the refinement study (1 fine, 2 medium, 3 coarse), the safety factor has been set to $F_s = 1.25$. For a characteristic integral flow quantity f the GCI can then be calculated by the following equations. Herein the refinement factor r is calculated from the number of volume cells in the grids N.

$$GCI_{12} = F_s \cdot \left| \frac{f_2 - f_1}{1 - r^p} \right| \tag{1}$$

$$r \approx \left(\frac{N_1}{N_2} \right)^{\frac{1}{3}} \tag{2}$$

Table 1 shows the calculated GCI error bands based on the axial position of the flow separation X_{sep} and the average pressure in the recirculation area $p_{plateau}$ which are the flow characteristics that are most significant to the structural loads. For the simulated NPR the error lies within a range of approximately six percent.

The element size of the CSM mesh was chosen small enough so that approximately ten elements lie within one axial wave (see figure 5). A preliminary modal analysis (see section 3) with CSM meshes of different spatial resolution has shown that a further refinement of the chosen discretization has no significant influence on the shape or frequency of the structural eigenmodes.

DOI: 10.13009/EUCASS2017-206

Analogue to the CSM element size, the physical timestep has been chosen small enough to resolve the axial waves along the nozzle surface. A complete resolution study for the timestep size has not been carried out due to its immense numerical costs. Single ongoing comparative calculations with a decreased timestep however show no notable influence onto the stability behaviour.

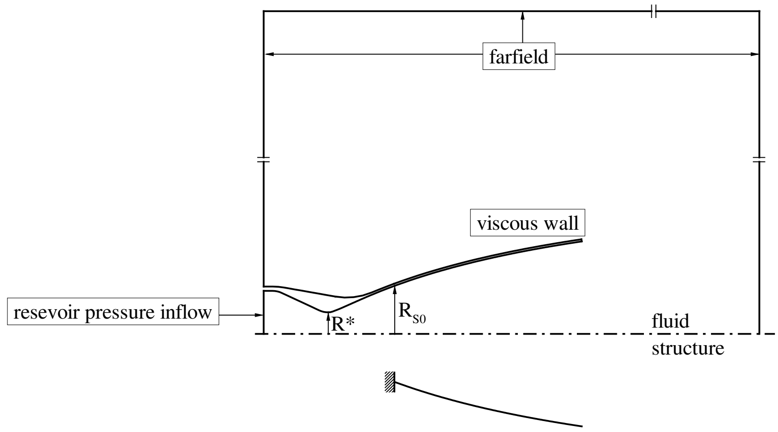

Figure 2: Cross section of the computational domain and boundary conditions

Table 1: Grid convergence index for different nozzle pressure ratios

NPR	$\Delta X_{sep}/l_{div}$	$\Delta p_{plateau}/p_a$
20	3.99 %	1.25 %
30	6.01 %	0.11 %
35	6.08 %	1.31 %

3. Modal analysis and scalability considerations

To reduce the problems complexity and to make underlying effects observable and especially measurable, the present work, as well as all preceding investigations, have focussed on subscale TIC nozzles. While other authors (e.g. Östlund[19] or Frey[6]) have proven that these assumptions are valid to investigate the effects within the fluid domain, there is little comparable unrestricted information available for the structural properties of rocket engine nozzles.

The geometry and eigenmode information of the Vulcain nozzle extension prototype HM60 published by Nyden and Rosendahl[18] has been used as a reference for scalability considerations. Similar to the used structure mesh, the geometry has been modelled by shell elements with a constant analogue thickness. To compensate for the neglected stiffeners and hollow tube structure the shell thickness has been increased until the eigenfrequencies fit the reference values. Large deviations between the analogue model and the published data are observed for the bending mode (figure 3a). Figure 3b shows the influence of the chosen wallthickness onto the eigenfrequencies of the modes analyzed by Nyden and Rosendahl, where n and m are the axial and the circumferential wavenumber of each eigenmode. For comparison, the used shell thickness has been normalized to the HM60's structure thickness and the resulting eigenfrequencies have been normalized to the experimental ones resulting in the dimensionless properties $\delta = t_w/t_{\text{tubes,HM60}}$ and $\Phi = f_{\text{analogue}}/f_{\text{orig,HM60}}$. An analogue shell thickness of $\delta = 10$ shows the smallest overall deviations and was therefore chosen for the following comparisons. While the eigenfrequencies of the ovalization and triangulization strongly depend on the analogue thickness, the bending modes frequency is nearly constant. Its eigenfrequency is dominated by the design of the clamping interface. At this interface, i.e. the upstream structural boundary condition, the original HM60 design has a complex load transmitting cone. The much simpler model of a clamped shell is not able to reproduce this behaviour. Besides this principal deviation, the analogue model reproduces the general structural properties and was therefore used for scalability considerations.

The dashed lines in figure 4a show the scaled eigenfrequencies of the TIC-53 compared to those of the HM60 nozzle. Scaling has been calculated by the ratio of the residence times of a flow particle in the flexible nozzle section assuming that this time is an indicator for the flows response time (analogue to the Stanton number for oscillating

DOI: 10.13009/EUCASS2017-206

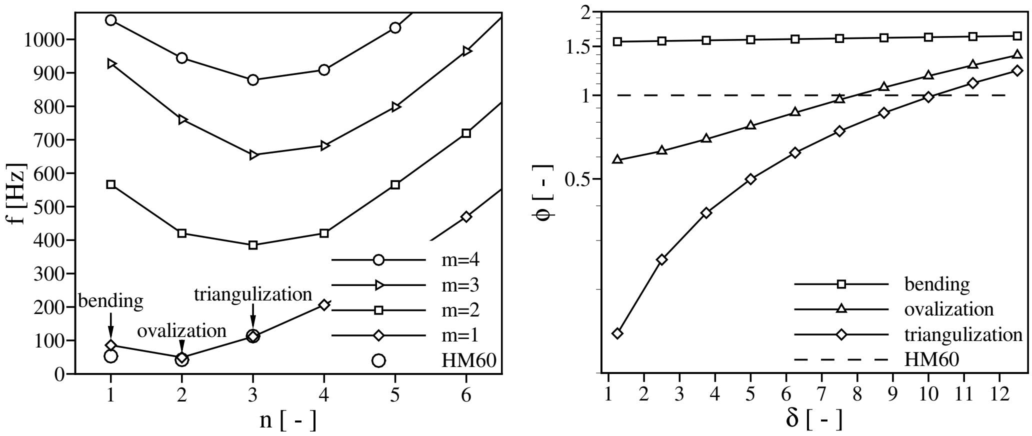

(a) (b)

Figure 3: Comparison of original[18] and analogue model results (a) and wall thickness influence on the eigen frequency (b) for the HM60 nozzle extension

flows). The shape of the frequency distributions is qualitatively the same, with the minimum eigenfrequency at $n = 2$ and $m = 1$, indicating that the HM60's structural properties are reproduced by the scaled nozzle. A comparison to validated analytical investigations by Arnold and Warburton[2] shows that this kind of frequency distribution is typical for free ended thin cylindrical structures. Based on these preliminary studies a quasi-isotropic glass-fiber reinforced plastic laminate (GFP) with a fiber volume ratio of 43 % has been chosen for all coupled simulations using the mechanical properties given in table 2.

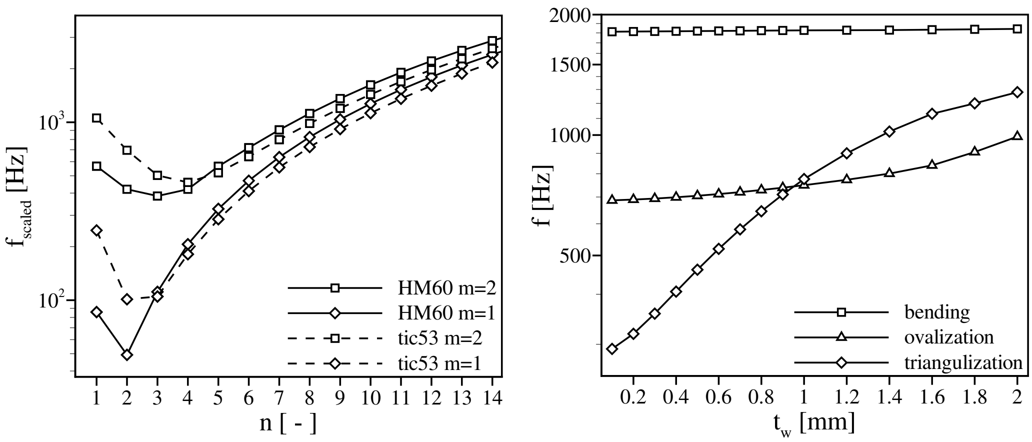

(a) (b)

Figure 4: Comparison of HM60 analogue model results with tic53 model (a) and wall thickness influence on the eigen frequency (b) for the tic53 nozzle

Table 2: Mechanical properties for GFP with a fiber volume ratio of 43 % as published by Swiss Composites[3]

elastic modulus	**Poisson's ratio**	**density**
E	ν	ρ
2.0×10^{10} Pa	0.18	2100 kg m^{-3}

DOI: 10.13009/EUCASS2017-206

4. Coupled simulations

The internal separation shock in the overexpanded nozzle flow leads to a steep local wall pressure gradient. During the first timesteps of a coupled simulation, this gradient leads to a local deformation as shown for NPR = 30, $t_w = 1.0\,\text{mm}$ in the upper half of figure 5. This resulting deformation then produces an axial wave that moves along the nozzle wall in up- and downstream direction. Cyclic deformations of the contour radius induced by these waves cause local oscillating changes in the nozzle wall pressure.

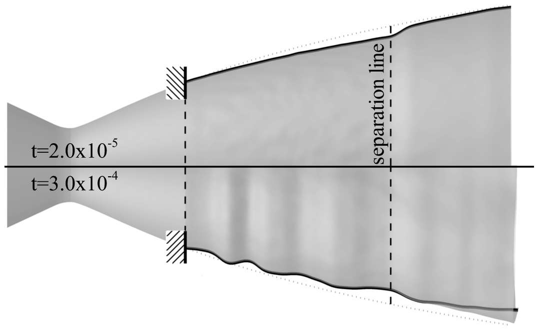

Figure 5: Sketch of the mechanism that leads to the running axial waves

Since the pressure and the exciting deformation feature a position-dependent phaseshift the fluid performs work on the wall structure. This local phase shift, the sign of the resulting pressure gradient and hence the performed work tend to damp the inital load mechanism in the supersonic region of the nozzle and excite it in the subsonic flow in the recirculation area as described in detail by Génin et al.[8] Figure 6a shows the total sum of the work that the fluid performs on the structure. This work has been calculated as the scalar product of the displacement and the load vector $W = df$ and summed over all fluid interface nodes. The black, red and green lines represent this total work W for the three wall thicknesses $t_w = 1.0\,\text{mm}$, $t_w = 1.5\,\text{mm}$ and $t_w = 2.0\,\text{mm}$ within the first eleven miliseconds of each calculation. For all shown cases exponential functions (dashed lines) $c\,\exp(\Lambda t)$ have been fitted to the transient data (solid lines). The slope of the fitted functions Λ can be used to evaluate the longtime stability of the coupled system. Figure 6b shows the functions' slopes , comparable to the logarithmic decrement of a damped harmonic oscillator. A postive sign of Λ means that the fluid performs work on the structure while a negative one indicates a damping function of the inner flow. The shown distribution points to a stability limit at a shell thickness between $t_w = 1.25\,\text{mm}$ and $t_w = 1.4\,\text{mm}$ depending on the nozzle pressure ratio.

As stated before, all simulations with a structure shell thickness of $t_w = 1.0\,\text{mm}$ represented an unstable coupled system. Figure 7a shows the isometric view onto the nozzle's inner wall at $t = 14.5\,\text{ms}$ for NPR = 30. All deformations in this figure have been amplified by a factor of three to emphasize its shape. The aforementioned axial waves and the resulting loading of the structure lead to a cyclic excitation of the nozzles triangulization eigenmode. This eigenmode has an eigenfrequency of 776.4 Hz, as shown in figure 4a. For the three surface nodes (A,B,C) indicated in figure 7a, the deformation history has been analyzed performing a fast Fourier transformation (FFT). Point A was chosen close to the local maximum, B close to the nodal line of the deformation, both close to the nozzle exit area. For comparison point C was chosen near the structure's clamping boundary condition. All computed amplitudes were normalized to the maximum occuring amplitude. Besides small chaotic ones, the frequency spectrum shows two distinct peeks. One of them, at a frequency of approximately 9 kHz represents the moving axial waves described in figure 5. At this point all of the processed points have comparable amplitudes, the wave moves along the nozzle wall with a nearly constant shape. The second peak at 550 Hz is caused by the excited triangular mode of the structure. The fluid structure coupling shifts the observed frequency of the triangulization to lower values compared to the vacuum, i.e. the modal, analysis. For this large-scale oscillation the calculated amplitude depends on the node position and is highest at point A.

DOI: 10.13009/EUCASS2017-206

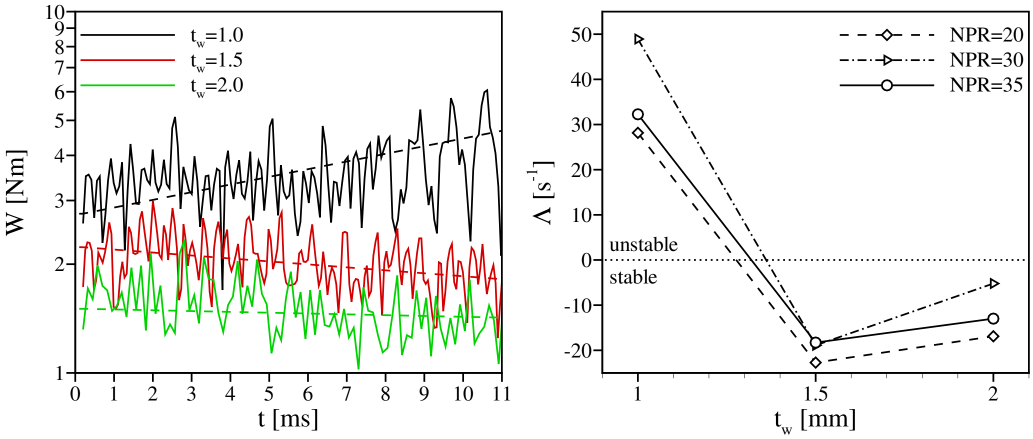

(a) (b)

Figure 6: Work performed by fluid on structure for NPR = 30 and t_w = 1.0 mm (a) and logarithmic decrement (b) for the tic53 nozzle

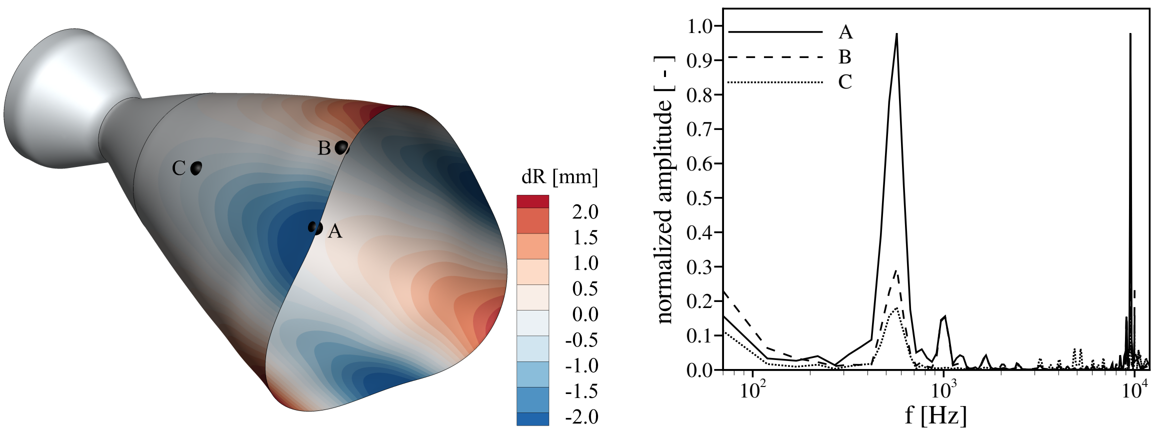

(a) (b)

Figure 7: Isometric view of the nozzle's inner wall for NPR = 30, t_w = 1.0 mm and t = 14.5 ms (a) and amplitude over frequency of the deformation (b) for the tic53 nozzle

5. Conclusion

Proceeding earlier studies of undeformed and stiff deformed subscale rocket engine nozzles, a partitioned coupled simulation environment using the DLR CFD solver TAU and the structural simulation tool MSC Nastran has been enhanced to simulate the fluid structure interaction in sub-scale rocket engine nozzles. To evaluate the mechanical properties of the nozzles structure a modal analysis has been performed to compare the results to literature data of the Vulcain nozzle extension prototype HM60, chosen as a realistic application case. The comparison shows good qualitative agreement for the eigenmodes' frequency distribution and values when a scaling with characteristic flow patterns is applied. Larger deviations do occur for the bending mode which are caused by the models simplified boundary condition. Coupled simulations show that the choice of the boundary conditions excites moving axial deformation waves. Although this excitation would be altered and reduced by the pressure transient during a realistic rocket engines start-up it serves as loading process for the large-scale oscillating triangular deformation. By altering the nozzles wall thickness the damping of the coupled system can be increased until it reaches a stable condition. The chosen sub scale nozzle model is assumed to be manufactured from glass-fiber reinforced plastic with a wall thickness of at least 1.0 mm with relevant structural and aeroelastic eigenfrequencies below 2.0 kHz. Both scales seem realistic to produce and measure within a testbench environment.

DOI: 10.13009/EUCASS2017-206

6. Acknowledgments

The presented work was part of the ongoing DLR internal cooperation project TAUROS.

References

[1] Marko Alder. Development and Validation of a Fluid–Structure Solver for Transonic Panel Flutter. *AIAA Journal*, 53(12):3509–3521, December 2015.

[2] R. N. Arnold and G. B. Warburton. The Flexural Vibrations of Thin Cylinders. *Proceedings of the Institution of Mechanical Engineers*, 167(1):62–80, 1953.

[3] Swiss Composite. GFK Werkstoffdaten.

[4] B.J. Daly and F.H. Harlow. Transport Equations in Turbulence. *Physics of Fluids*, 13:2634–2649, 1970.

[5] Tomas Damgaard, Jan Östlund, and Manuel Frey. Side-Load Phenomena in Highly Overexpanded Rocket Nozzles. *Journal of Propulsion and Power*, 20(4):695–704, July 2004.

[6] Manuel Frey. *Behandlung von Strömungsproblemen in Raketendüsen bei Überexpansion*. PhD thesis, Universität Stuttgart, Stuttgart, 2001.

[7] Chloé Génin and Sebastian Jack. Flow Separation Study in Stiff Ovalized Rocket Nozzles, Part I: Experimental Approach. Orlando, USA, July 2015. American Institute of Aeronautics and Astronautics.

[8] Chloé Génin, Sebastian Jack, and Ralf Stark. Flow Visualization in Out-of-Round Rocket Nozzles. Tel Aviv, Israel, 2015.

[9] Chloé Génin, Ralf Stark, and Sebastian Jack. Flow Separation in Out-of-Round Nozzles, a Numerical and Experimental Study. *Progress in Flight Physics*, 7:269–282, 2015.

[10] Hans M. Hilber, Thomas J. R. Hughes, and Robert L. Taylor. Improved Numerical Dissipation for Time Integration Algorithms in Structural Dynamics. *Earthquake Engineering Structural Dynamics*, 5(3):283–292, 1977.

[11] Sebastian Jack and Chloé Génin. Numerical and Experimental Investigation of Flow Separation in Ovalized Nozzles. Köln, 2014.

[12] Sebastian Jack and Chloé Génin. Flow Separation Study in Stiff Ovalized Rocket Nozzles, Part II: Numerical Approach. Orlando, USA, July 2015. American Institute of Aeronautics and Astronautics.

[13] Antony Jameson. Application of Dual Time Stepping to Fully Implicit Runge Kutta Schemes for Unsteady Flow Calculations. In *22nd AIAA Computational Fluid Dynamics Conference*, page 2753, 2015.

[14] B.E. Launder, G.J. Reece, and W. Rodi. Progress in the Development of a Reynolds-Stress Turbulent Closure. *Journal of Fluid Mechanics*, pages 537–566, 1975.

[15] F.R. Menter. Multiscale Model for Turbulent Flows. Orlando, USA, 1993.

[16] MSC. MSC Nastran 2014 Nonlinear User's Guide, November 2014.

[17] Jens Neumann. Identifikation radialer Basisfunktionen zur räumlichen Strömung-Struktur-Kopplung unter Berücksichtigung des Interpolations- und des Lasttransformationsfehlers. Technical report, January 2008.

[18] O. Nyden and B. Rosendahl. Development of the HM60-Vulcain Nozzle Extension. American Institute of Aeronautics and Astronautics, June 1991.

[19] Jan Östlund. *Flow Processes in Rocket Engine Nozzles with Focus on Flow Separation and Side-Loads*. PhD thesis, KTH Royal Institute of Technology, Stockholm, 2002.

[20] M. Rakowitz. Grid Refinement Study with a UHCA Wing-Body Configuration Using Richardson Extrapolation and Grid Convergence Index GCI. *New Results in Numerical and Experimental Fluid Mechanics III*, pages 297–303, 2002.

[21] Patrick J. Roache. Quantification of Uncertainty in Computational Fluid Dynamics. *Annual review of fluid Mechanics*, 29(1):123–160, 1997.

[22] J. Rotta. Statistische Theorie nichthomogener Turbulenz. *Zeitschrift für Physik*, 129(6):547–572, 1951.